ELSEVIER

Journal of Materials Processing Technology 123 (2002) 47–53

Journal of Materials Processing Technology

www.elsevier.com/locate/jmatprotec

Extrusion of three-layer composite hexagonal clad rods

C.W. Wu[a,*], R.Q. Hsu[b]

[a]*Institute of Applied Mechanics, National Taiwan University, No. 1, Sec. 4, Roosevelt Road, Taipei, Taiwan, ROC*
[b]*Department of Mechanical Engineering, National Chiao Tung University, 1001 Ta-Hsueh Road, Hsinchu, Taiwan, ROC*

Received 10 February 2001

Abstract

Composite clad rods consisting of three different materials are applied extensively as conductors, electrodes and chemical devices. Commercial applications involving low temperature niobium–tin alloy (Nb_3Sn) superconductor rods, which have a pure niobium (Nb) core, a copper–tin (Cu–Sn) alloy outer sleeve and a Nb_3Sn diffusion layer in between, stipulate these conductors as, electrodes that are intended for processing as rods of various shapes. During the extrusion process, non-homogeneous deformation tends to occur because the billet consists of materials with different mechanical properties. In this study, the authors present a numerical simulation model based on the upper-bound theorem to analyze three-layer composite clad rods with a hexagonal cross-section under extrusion. A velocity field is also generated with the assistance of a product's cross-section profile functions. The velocity component in the extrusion axis is expressed as a convex distribution. Analytical results indicate that various process variables such as the semi-die angle, reduction of area, friction condition of the die and combinations of the three constituent materials, prominently influence the extrusion process. Moreover, the extrusion pressure, product dimension-change and the probability of sound extrusion are related closely to the process variables.

Keywords: Composite clad rods; Niobium–tin alloy; Copper–tin alloy

1. Introduction

Composite clad rods having received increasing attention owing to their diverse applications in fields such as electronics, nuclear engineering and chemistry. In addition to conventional composite rods which consist of two distinct constituents, the market demand for increasingly complicated composite clad rods is the increase also. For instance, three-layer composite clad rods are used commercially as superconductor cables, with pure niobium as the core, copper–tin alloy as the sleeve and a Nb_3Sn diffusion layer in between. Similarly to the manufacturing of conventional composite clad rods, these three-layer composite clad rods are extruded from a billet consisting of three distinct constituents. During the extrusion process, owing to the differences among mechanical properties with respect to the constituent materials and the complexity of construction, three-layer composite clad rods frequently exhibit a non-homogeneous deformation in the extrusion process, subsequently leading to fracturing or defects within the core, the mid-layer and the sleeve.

The extrusion of conventional composite clad rods consisting of two constituents has been examined thoroughly [1–8]. These studies focused primarily on bi-metal rods, in which analytical models were developed subsequently, but which are applicable only to two-layer composite clad rods. Studies involving the rolling of a sandwich plate (which also has three layers) closely examined the problem's complexity [9]. Although the authors' earlier work proposed an analytical model to extrude a three-layer composite rod [10], the extrusion was confined to axisymmetric round rods.

In this study, the authors refine the above model to extrude three-layer composite clad rods with hexagonal cross-sectional profiles. Also proposed herein is a three-dimensional velocity field which has a non-uniform velocity distribution in the extrusion axis. In addition, the deformation behavior of each layer during extrusion is examined.

2. Formulation of velocity field

Fig. 1 depicts schematically the extrusion of a hexagonal three-layer composite clad rod. The round billet deforms to the final hexagonal cross-section through the die, which is defined by an envelope of a number of straight lines. The composite clad rod consists of a core, a mid-layer and an outer sleeve.

* Corresponding author. Tel.: +886-2-23654370; fax: +886-2-23639290.
E-mail address: cwwu@nscmems.iam.ntu.edu.tw (C.W. Wu).

0924-0136/02/$ – see front matter
PII: S0924-0136(02)00036-5

Nomenclature

A_s	area of the sleeve at the die exit
D_s, D_m, D_c	non-uniform velocity component in the extrusion axis of the sleeve, mid-layer and core, respectively
J	total power consumption in extrusion
L	die length (dimensionless)
m, $m1$, $m2$	friction factor at the die surface, mid-layer/sleeve and core/mid-layer inter-surface, respectively
P_{avg}	average extrusion pressure
r, ϕ, y	cylindrical coordinates
$R_f(\phi)$	product radius function
R_f, R_{mf}, R_{cf}	radius of the sleeve, mid-layer and core after extrusion, respectively
R_{ss}, R_{sm}, R_{sc}	functions represents the die surface, mid-layer/sleeve and core/mid-layer inter-surface profile, respectively
R_0, R_{m0}, R_{c0}	radius of the sleeve, mid-layer and core before extrusion, respectively
RA	reduction of area of the billet
$\partial R_{ss}/\partial_y$, $\partial R_{sm}/\partial_y$, $\partial R_{sc}/\partial_y$	first derivative of die surface, mid-layer/sleeve and core/mid-layer inter-surface profile functions with respect to y, respectively
U_s, U_m, U_c	uniform velocity component in the extrusion axis of the sleeve, mid-layer and core, respectively
$\partial U_s/\partial_y$, $\partial U_m/\partial_y$, $\partial U_c/\partial_y$	first derivative of the uniform velocity component in the extrusion axis of the sleeve, mid-layer and core with respect to y, respectively
V_p	volume of the plastic region
V_{rc}, $V_{\phi c}$, V_{yc}	velocity components of the core in cylindrical coordinates (r, ϕ, y), respectively
V_{rm}, $V_{\phi m}$, V_{ym}	velocity components of the mid-layer in cylindrical coordinates (r, ϕ, y), respectively
V_{rs}, $V_{\phi s}$, V_{ys}	velocity components of the sleeve in cylindrical coordinates (r, ϕ, y), respectively
V_0, V_{fs}, V_{fm}, V_{fc}	entrance velocity of the billet, exit velocity of sleeve, mid-layer and core of the extruded product, respectively
$\Delta V_{\Gamma_s}, \Delta V_{\Gamma_f}$	relative slip velocity on the Γ_s and Γ_f surfaces, respectively
$\dot{W}_i, \dot{W}_s, \dot{W}_f$	power dissipation due to internal deformation, internal shear and friction, respectively
$\dot{W}_{ic}, \dot{W}_{sc}, \dot{W}_{f2}$	power dissipation due to internal deformation, internal shear of the core and friction at the core/mid-layer inter-surface, respectively
$\dot{W}_{im}, \dot{W}_{sm}, \dot{W}_{f1}$	power dissipation due to internal deformation, internal shear of the mid-layer and friction at the mid-layer/sleeve surface, respectively
$\dot{W}_{is}, \dot{W}_{ss}, \dot{W}_{fd}$	power dissipation due to internal deformation, internal shear of the sleeve and friction at the die surface, respectively
Y_{ss}, Y_{sm}, Y_{sc}	yield stress of the sleeve, mid-layer and core, respectively
Z_s, Z_m, Z_c	functions of (β_s, R_{ss}, L), (β_m, R_{sm}, L) and (β_c, R_{sc}, L), respectively
$\partial Z_s/\partial_y$, $\partial Z_m/\partial_y$, $\partial Z_c/\partial_y$	first derivative of functions Z_s, Z_m, Z_c with respect to y, respectively

Greek symbols

α	semi-die angle
Γ_s, Γ_f	surface of shear velocity discontinuities and friction, respectively
δ, λ, β_s, β_m, β_c	optimization parameters introduced in the velocity fields
σ_0, $\dot{\bar{\varepsilon}}$	the yield stress and effective strain rate of the materials, respectively
$\phi_f(y)$	angle of a surface of geometric symmetry
ω_s, ω_m, ω_c	angular velocity of the sleeve, mid-layer and core, respectively
$\partial\omega_s/\partial\phi$	first derivative of the angular velocity of sleeve with respect to ϕ

Each layer of the rod has a circular cross-section before extrusion. Following extrusion, the die used dictates the cross-sectional shape of the composite clad rod. In this study, the authors thoroughly examine a non-axisymmetric product with a hexagonal cross-section. For simplicity, the following assumptions are made to establish a three-dimensional velocity field that describes the materials flow in each layer:

1. All constituent layers of the rod are made of isotropic, homogeneous, and rigid–plastic materials.
2. The die is assumed to be rigid throughout the extrusion process.
3. Heat affect are neglected in the analysis.
4. Plastic deformation occurs only within zones bounded by the die entrance plane (A–A′), the die exit plane, (B–B′) and the die surface, as indicated in Fig. 2. Before entering the die, the composite clad rod moves as a rigid body with the same velocity V_0, in the extrusion direction; whilst after extrusion, each layer of the composite clad rod may move with different velocity V_{fs}, V_{fm} and V_{fc} if non-homogeneous deformation occurs.
5. The core and the mid-layer remain circular after extrusion while outer sleeve cross-section is completely defined by the die profile. During the analysis, the material characteristics determine the interfacial boundaries.

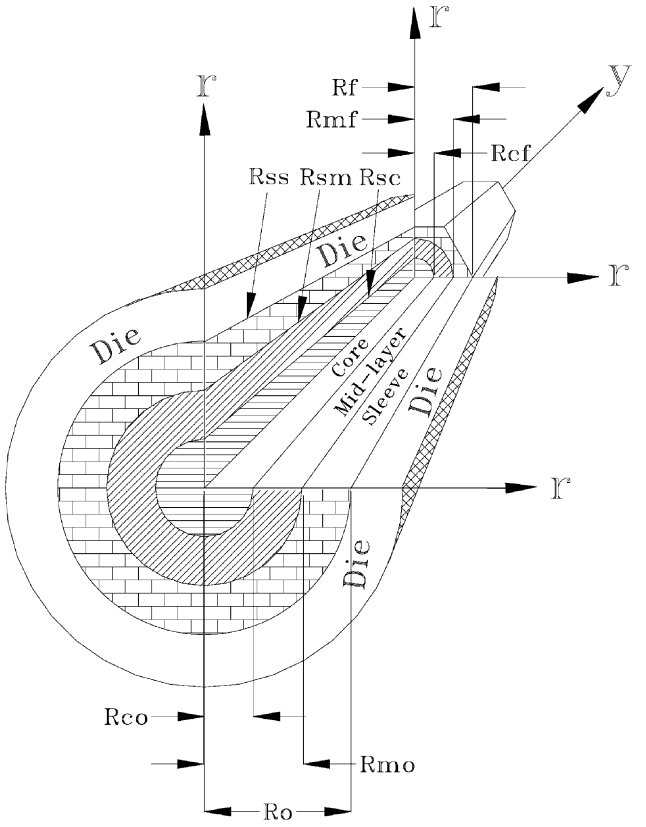

Fig. 1. Schematic representation of the extrusion of a three-layer composite clad rod with a hexagonal cross-sectional profile.

Fig. 2 illustrates a three-layer composite clad rod that is being extruded through a linearly converging die. Each constituent layer has its own material characteristics, accounting for why a particular velocity field must be developed for each layer. Initially, the polar coordinate system (r, ϕ, y) is imposed with its origin selected at the center of the billet at the die entrance plane. The y-axis is aligned with the extrusion axis. Before entering the die entrance, the billet is pushed forward, each layer of the composite rod moving with the same entrance speed V_0. After entering the die entrance plane, the composite rod starts to deform. Herein, for each constituent layer, a convex distributed non-uniform V_y with specific parameter β_s, β_m, β_c, is introduced to control its convexity. On the other hand, a rotational velocity component V_ϕ exists since the outer sleeve experiences non-axisymmetric deformation. Furthermore, it is assumed that V_ϕ is linearly distributed over the radius, i.e. $V_\phi = r\omega(\phi, y)$. At the same time the angular velocity $\omega_c(\phi, y)$, $\omega_m(\phi, y)$ of the core and the mid-layer are zero owing to the core and the mid-layer remaining circular after extrusion, and thus both are axisymmetrical. In addition, the three-dimensional admissible velocity fields for the core, the mid-layer, and the sleeve can be derived with the assistance of incompressibility of materials or constant volume flow. These results are summarized below.

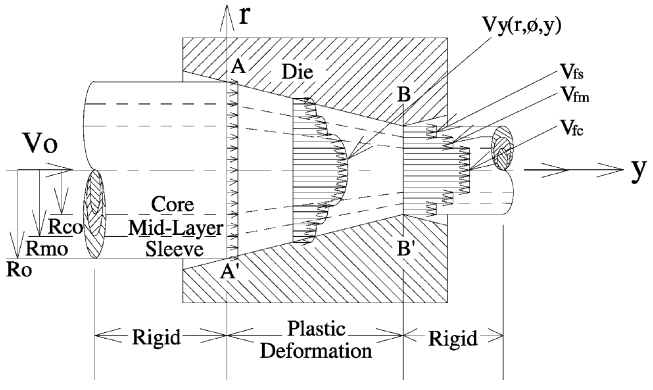

Fig. 2. Velocity components in the extrusion direction (the y-axis).

(a) Velocity of the sleeve:

$$V_{ys}(r,\phi,y) = D_s(r,\phi,y)U_s(y) \tag{1}$$

$$V_{\phi s}(r,\phi,y) = r\omega_s(\phi,y) \tag{2}$$

$$\begin{aligned} V_{rs}(r,\phi,y) = &-\frac{r}{2}\left[\frac{\partial U_s(y)}{\partial y} + \frac{\partial \omega_s(\phi,y)}{\partial \phi}\right] \\ &+ \frac{r^3}{4}\left[Z_s(\phi,y)\frac{\partial U_s(y)}{\partial y} + U_s(y)\frac{\partial Z_s(\phi,y)}{\partial y}\right] \\ &- \frac{1}{r}\left\{\frac{R_{sm}^4(\phi,y)}{4}\left[Z_s(\phi,y)\frac{\partial U_s(y)}{\partial y} + U_s(y)\frac{\partial Z_s(\phi,y)}{\partial y}\right]\right. \\ &- \frac{R_{sm}^2(\phi,y)}{2}\left[\frac{\partial U_s(y)}{\partial y} + \frac{\partial \omega_s(\phi,y)}{\partial \phi}\right] \\ &\left. - V_{ys}(R_{sm}(\phi,y),\phi,y)R_{sm}(\phi,y)\frac{\partial R_{sm}(\phi,y)}{\partial y}\right\} \end{aligned} \tag{3}$$

Here

$$D_s(r,\phi,y) = 1 - \frac{4\beta_s y(L-y)}{R_{ss}^2(\phi,y)L^2}r^2,$$

$$Z_s(\phi,y) = \frac{4\beta_s y(L-y)}{R_{ss}^2(\phi,y)L^2} \tag{4}$$

$$U_s(y) = \frac{V_0\int_0^{\phi_f(0)}[R_{ss}^2(\phi,0) - R_{sm}^2(\phi,0)]\,d\phi}{\int_0^{\phi_f(y)}\left[R_{ss}^2(\phi,y) - R_{sm}^2(\phi,y) - Z_s(\phi,y)\frac{R_{ss}^4(\phi,y) - R_{sm}^4(\phi,y)}{2}\right]d\phi} \tag{5}$$

$$\begin{aligned} \omega_s(\phi,y) = &\frac{-2}{R_{ss}^2(\phi,y) - R_{sm}^2(\phi,y)} \\ &\times \int_0^{\phi_f(y)}\left[V_{ys}(R_{ss}(\phi,y),\phi,y)R_{ss}(\phi,y)\frac{\partial R_{ss}(\phi,y)}{\partial y}\right. \\ &- V_{ys}(R_{sm}(\phi,y),\phi,y)R_{sm}(\phi,y)\frac{\partial R_{sm}(\phi,y)}{\partial y} \\ &+ \left[\frac{R_{ss}^2(\phi,y) - R_{sm}^2(\phi,y)}{2} - Z_s(\phi,y)\frac{R_{ss}^4(\phi,y) - R_{sm}^4(\phi,y)}{4}\right] \\ &\left.\times \frac{\partial U_s(y)}{\partial y} - \frac{R_{ss}^4(\phi,y) - R_{sm}^4(\phi,y)}{4}\frac{\partial Z_s(\phi,y)}{\partial y}U_s(y)\right]d\phi \end{aligned} \tag{6}$$

(b) Velocity of the mid-layer:

$$V_{ym}(r,\phi,y) = D_m(r,\phi,y)U_m(y) \tag{7}$$

$$V_{\phi m}(r,\phi,y) = r\omega_m(\phi,y) = 0 \tag{8}$$

$$\begin{aligned} V_{rm}(r,\phi,y) &= -\frac{r}{2}\frac{\partial U_m(y)}{\partial y} + \frac{r^3}{4}\left[Z_m(\phi,y)\frac{\partial U_m(y)}{\partial y} + U_m(y)\frac{\partial Z_m(\phi,y)}{\partial y}\right] \\ &\quad - \frac{1}{r}\left\{\frac{R_{sc}^4(\phi,y)}{4}\left[Z_m(\phi,y)\frac{\partial U_m(y)}{\partial y} + U_m(y)\frac{\partial Z_m(\phi,y)}{\partial y}\right]\right. \\ &\quad - \frac{R_{sc}^2(\phi,y)}{2}\frac{\partial U_m(y)}{\partial y} \\ &\quad \left. - V_{ym}(R_{sc}(\phi,y),\phi,y)R_{sc}(\phi,y)\frac{\partial R_{sc}(\phi,y)}{\partial y}\right\} \end{aligned} \tag{9}$$

Here

$$D_m(r,\phi,y) = 1 - \frac{4\beta_m y(L-y)}{R_{sm}^2(\phi,y)L^2}r^2,$$

$$Z_m(\phi,y) = \frac{4\beta_m y(L-y)}{R_{sm}^2(\phi,y)L^2} \tag{10}$$

$$U_m(y) = \frac{V_0\int_0^{\phi_f(0)}[R_{sm}^2(\phi,0) - R_{sc}^2\phi,0]\,d\phi}{\int_0^{\phi_f(y)}\left[R_{sm}^2(\phi,y) - R_{sc}^2(\phi,y) - Z_m(\phi,y)\frac{R_{sm}^4(\phi,y) - R_{sc}^4(\phi,y)}{2}\right]d\phi} \tag{11}$$

(c)Velocity of the core:

$$V_{yc}(r,\phi,y) = D_c(r,\phi,y)U_c(y) \tag{12}$$

$$V_{\phi c}(r,\phi,y) = r\omega_c(\phi,y) = 0 \tag{13}$$

$$V_{rc}(r,\phi,y) = -\frac{r}{2}\frac{\partial U_c(y)}{\partial y} + \frac{r^3}{4}\left[Z_c(\phi,y)\frac{\partial U_c(y)}{\partial y} + U_c(y)\frac{\partial Z_c(\phi,y)}{\partial y}\right] \tag{14}$$

Here

$$D_c(r,\phi,y) = 1 - \frac{4\beta_c y(L-y)}{R_{sc}^2(\phi,y)L^2}r^2,$$

$$Z_c(\phi,y) = \frac{4\beta_c y(L-y)}{R_{sc}^2(\phi,y)L^2} \tag{15}$$

$$U_c(y) = \frac{V_0\int_0^{\phi_f(0)}R_{sc}^2(\phi,0)\,d\phi}{\int_0^{\phi_f(y)}\left[R_{sc}^2(\phi,y) - Z_c(\phi,y)\frac{R_{sc}^4(\phi,y)}{2}\right]d\phi} \tag{16}$$

Herein, the velocity components for the core, the mid-layer and the sleeve in the extrusion axis, V_{yc}, V_{ym} and V_{ys} are assumed to consist of a uniform component U_s, U_m, U_c, and a non-uniform component D_s, D_m, D_c, respectively. Notably, $R_{ss}(\phi, y)$, $R_{sm}(\phi, y)$ and $R_{sc}(\phi, y)$ are functions that describe the die surface, the mid-layer/sleeve and the core/mid-layer inter-surfaces, respectively. In the case of a linearly converging die, the following equations represent these functions:

$$R_{ss}(\phi,y) = \left\{R_0 - \left[(R_0 - R_f(\phi))\frac{y}{L}\right]\right\} \tag{17}$$

$$R_{sm}(\phi,y) = \left\{R_{m0} - \left[(R_{m0} - R_{mf})\frac{y}{L}\right]\right\} \tag{18}$$

$$R_{sc}(\phi,y) = \left\{R_{c0} - \left[(R_{c0} - R_{cf})\frac{y}{L}\right]\right\} \tag{19}$$

In the above equations, R_0, R_{m0} and R_{c0} denote the radius of the sleeve, the mid-layer and the core before extrusion, respectively. During the extrusion process, since the core and the mid-layer are assumed to retain a circular cross-section, R_{mf} and R_{cf} are the radius of the mid-layer and of the core after extrusion, respectively. In addition, R_f is the dimension of the hexagonal length after extrusion as shown in Fig. 3. where L denotes the die length. One characteristic of this velocity field is that each velocity component can be directly calculated once the functions $R_{ss}(\phi,y), R_{sm}(\phi,y), R_{sc}(\phi,y)$ are defined. During the analysis, constant friction factors $m1$, $m2$ are adopted to calculate the friction energy loss on the core/mid-layer and mid-layer/sleeve inter-surfaces, respectively.

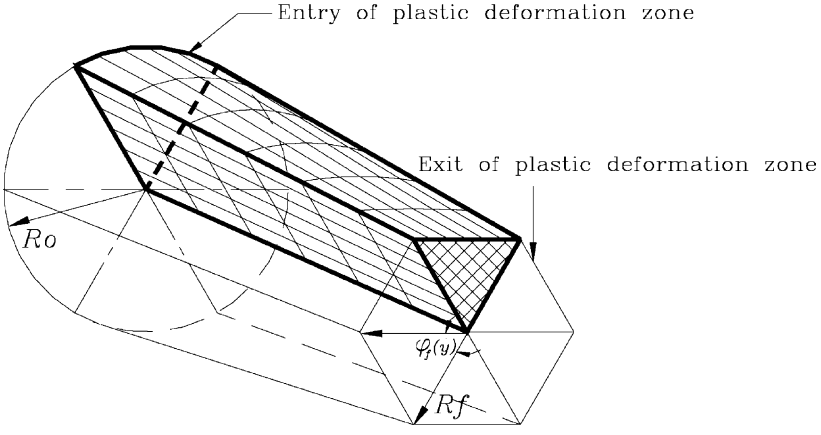

Fig. 3. Extrusion die for a hexagonal cross-section.

3. Optimal parameters

As mentioned earlier, each constituent layer may not deform homogeneously owing to their dissimilar mechanical properties. Under these circumstance, the reduction of each constituent layer may be different from that of the others. Thus, the exit radius ratios of the core/sleeve and mid-layer/sleeve differ from those of the assembled billet. Herein, parameters δ, λ are introduced to account for this non-homogeneous deformation, i.e.:

$$R_{\mathrm{mf}} = \left[\frac{(1+\delta)A_{\mathrm{s}}}{\pi}\right]^{1/2}\frac{R_{\mathrm{m0}}}{R_0}, \qquad R_{\mathrm{cf}} = \left[\frac{(1+\lambda)A_{\mathrm{s}}}{\pi}\right]^{1/2}\frac{R_{\mathrm{c0}}}{R_0} \tag{20}$$

where A_{s} is the area of sleeve at the die exit.

Minimizing the total extrusion power determines the value of parameter δ, λ. On the other hand, non-uniform velocity components in the y-axis, $D_{\mathrm{s}}(r, \phi, y)$, $D_{\mathrm{m}}(r, \phi, y)$, $D_{\mathrm{c}}(r, \phi, y)$ are specified by the parameters β_{s}, β_{m}, β_{c}, respectively.

Obviously, $V_{\mathrm{ys}}(r, \phi, y) = U_{\mathrm{s}}(y)$, $V_{\mathrm{ym}}(r, \phi, y) = U_{\mathrm{m}}(y)$, $V_{\mathrm{yc}}(r, \phi, y) = U_{\mathrm{c}}(y)$ at $y = 0$, L. Restated, the velocity components in the y-axis for all layers in both the die entrance and the die exit are uniformly distributed. Only in the plastic deformation zone, can $D_{\mathrm{s}}(r, \phi, y)$, $D_{\mathrm{m}}(r, \phi, y)$ and $D_{\mathrm{c}}(r, \phi, y)$ be non-zero functions. Thus δ, λ, β_{s}, β_{m}, β_{c} are considered as optimal parameters and their values are optimized mathematically by minimizing the total power J consumed in the extrusion process.

4. Power consumption

While extruding a hexagonal three-layer composite clad rod, the power consumption includes the power deemed necessary to overcome the resistance to deformation of the sleeve, the mid-layer and the core, $\dot{W}_{\mathrm{is}}, \dot{W}_{\mathrm{im}}, \dot{W}_{\mathrm{ic}}$; the shear power losses, $\dot{W}_{\mathrm{ss}}, \dot{W}_{\mathrm{sm}}, \dot{W}_{\mathrm{sc}}$ over boundaries of velocity discontinuities (slip), A–A′, B–B′; and frictional power consumed along the die surface, the mid-layer/sleeve and the core/mid-layer inter-surfaces, $\dot{W}_{\mathrm{fd}}, \dot{W}_{\mathrm{f1}}, \dot{W}_{\mathrm{f2}}$. This power consumption can be estimated by integrating the strain rate and the yield stress over the entire deformation volume. Each strain rate can be readily calculated from the velocity field formulated above. The formulations for the above mentioned power items are expressed as follows:

$$\dot{W}_{\mathrm{i}} = \int_{V_{\mathrm{p}}} \sigma_0 \dot{\bar{\varepsilon}}\, \mathrm{d}v \tag{21}$$

$$\dot{W}_{\mathrm{s}} = \int_{\Gamma_{\mathrm{s}}} \frac{1}{\sqrt{3}}\sigma_0 \Delta V_{\Gamma_{\mathrm{s}}}\, \mathrm{d}s \tag{22}$$

$$\dot{W}_{\mathrm{f}} = \int_{\Gamma_{\mathrm{f}}} \frac{m}{\sqrt{3}}\sigma_0 \Delta V_{\Gamma_{\mathrm{f}}}\, \mathrm{d}A \tag{23}$$

where σ_0 denotes the yield stress of the constituent materials; $\dot{\bar{\varepsilon}}$ represents the effective strain rate of the materials; V_{p} the volume of the plastic deformation region; $\Delta V_{\Gamma_{\mathrm{s}}}$ denotes the relative slip velocity at velocity discontinue surfaces; m represents the friction factor; and $\Delta V_{\Gamma_{\mathrm{f}}}$ the relative slip velocity at frictional surfaces.

5. Results and discussion

This study closely examines the extrusion of hexagonal three-layer composite clad rods from round billets. All of the dies used in the analysis are linearly connected and equiangularly divided, as indicated in Fig. 3. Herein, a semi-die angle is defined as the angle of die surface inclination.

Fig. 4 depicts the extrusion pressure required under several reduction ratios (RA) against semi-die angles. According to this figure, the pressure required becomes larger at small the semi-die angle. With an increasing semi-die angle, the extrusion pressure gradually decreases and then reaches a minimum. Beyond this angle, the extrusion pressure increases with further increase in semi-die angle. This tendency suggests that an optimal semi-die angle exists for the extrusion of a hexagonal three-layer composite clad rod. With small die angles, the lengths of contact between the billet and die are longer, causing significantly high friction losses, whilst with large die angles, although the die lengths are reduced, the internal deformation becomes a predominant factor. For the working conditions illustrated in this figure, the extrusion pressures are minimum at semi-die angles between 10° and 20°.

Fig. 5 depicts how the semi-die angle influences the exit radius of mid-layer, R_{mf}. In this case, the core has the highest yield stress, while sleeve has the lowest in the combination of the billet. Thus, the core is more resistant to deformation. In an extreme situation, the core acts as a mandrel, particularly at larger die angles, where the plastic flow is more severe. Therefore, the exit radius of the mid-layer tends to increase with an increase in semi-die angle, while at a smaller semi-die angle, the die angle does not affect R_{mf}.

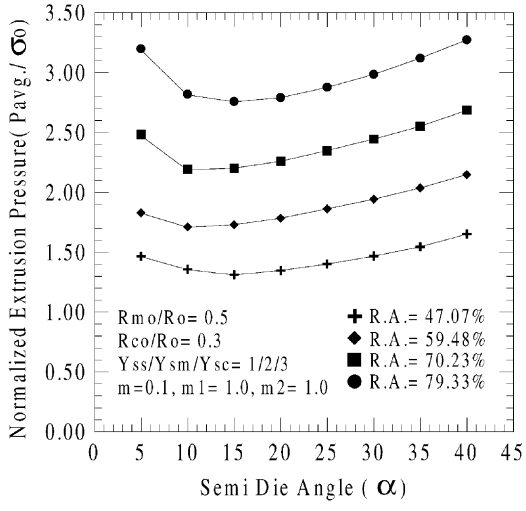

Fig. 4. Affects of the semi-die angle on the extrusion pressure.

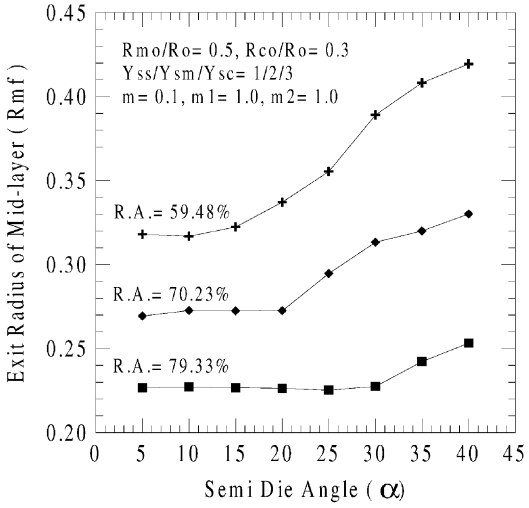

Fig. 5. Affects of the semi-die angle on the exit radius of the mid-layer.

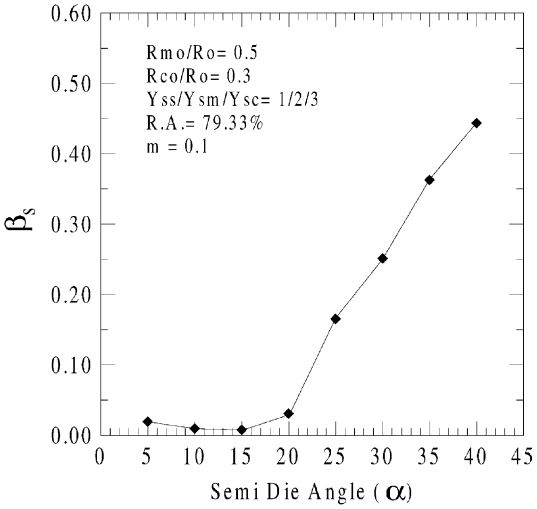

Fig. 7. Affects of semi-die angle of the die on β_s.

Fig. 6 plots the normalized extrusion pressure against the semi-die angle under three different die surface friction conditions. This figure indicates that the normalized extrusion pressure generally increases with an increase in friction factor. For the case where the friction factor is zero, no optimal semi-die angle exists, the reason being that when the frictional power is zero, the total extrusion pressure consists only of that for internal deformation and shear losses.

Fig. 7 displays parameter β_s which describes the degree of non-uniformity of velocity component V_{ys}, against the semi-die angle. A larger positive value of β_s implies that V_{ys} has a more prominent concavity distribution. In addition, a larger die surface friction factor implies a more sticky die surface. Under these circumstance, material flow along the extrusion axis is thus retarded on the die surface; therefore, β_s is larger. For a larger semi-die angle, while other process variables remain the same, the deformation is more severe. Moreover, the deviation of the velocity component along the extrusion axis for a greater semi-die angle exceeds that for a smaller semi-die angle. Thus, β_s increases with an increase in the semi-die angle. However, for an angle smaller than 20°, β_s approaches zero, i.e. the velocity component V_{ys} is almost uniform across the whole section.

Fig. 8 relates to two composite clad rods with different strength combinations. One of the clad rods has a harder sleeve and a softest mid-layer. whilst the other has a softer sleeve and a harder core. The fact that the volume of sleeve is the larger in both of the rods accounts for why a greater yield stress of the sleeve implies a greater extrusion pressure, as shown in Fig. 8.

Fig. 9 demonstrates that the strength-combination conditions affect the exit radii of the mid-layer and the core. For $Y_{ss}/Y_{sm}/Y_{sc} = 3/1/2$, the mid-layer and the core are more easily deformed, particularly at larger die angles where plastic flows are more severe. Therefore, the exit radius tends to decrease with an increase in the semi-die angle.

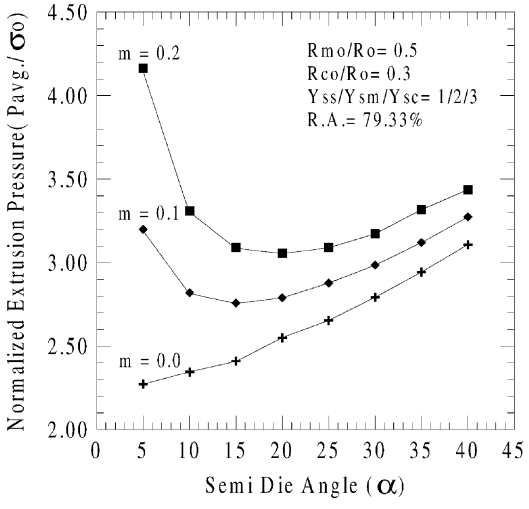

Fig. 6. Affects of friction factor of the die on the extrusion pressure.

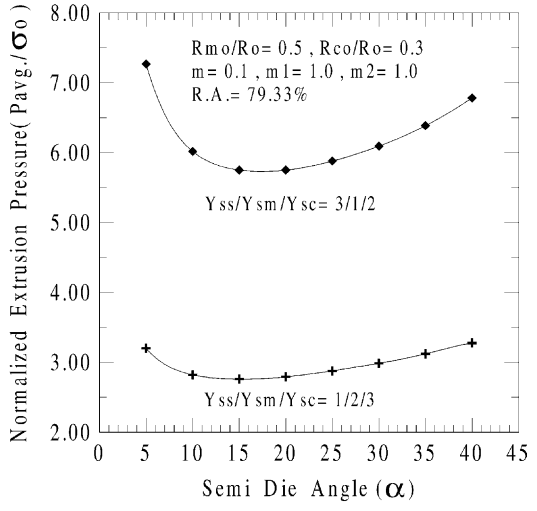

Fig. 8. Affects of the combination of the three-layer constituent materials on the extrusion pressure.

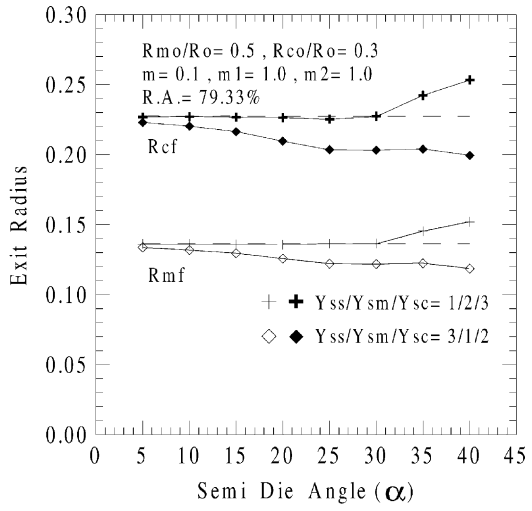

Fig. 9. Affects of the combination of the three-layer constituent materials on the exit radius.

On the other hand, for yield stress combination of $Y_{ss}/Y_{sm}/Y_{sc} = 1/2/3$, the exit radii of mid-layer and the core are quite steady against semi-die angle. However, when the semi-die angle exceeds 30°, these radii have a tendency to increase. Importantly, the deviation of either R_{cf} or R_{mf} from the dashed line denotes the degree of non-homogeneous flow of the billet.

Fig. 10 displays the non-homogeneity of the plastic flow of the billet. Owing to the billet being comprised of three materials, velocity differences exist in the core/mid-layer and in mid-layer/sleeve inter-surfaces. Only the larger velocity difference is selected for explanation in Fig. 10. Herein, the exit velocity difference of the two combinations of billets is shown against the semi-die angle. For $Y_{ss}/Y_{sm}/Y_{sc} = 1/2/3$, the exit velocity difference is nearly zero at angles smaller than 30°, i.e. the deformation of the billet is

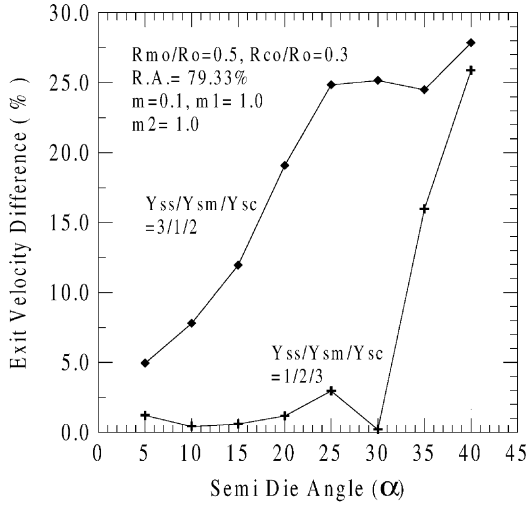

Fig. 10. Affects of the combination of the three-layer constituent materials on the exit velocity difference.

homogeneous. At angles larger than 30°, the exit velocity difference increases rapidly, indicating the tendency for unsound extrusion. On the other hand, for $Y_{ss}/Y_{sm}/Y_{sc} = 3/1/2$, the exit velocity difference increases with semi-die angle, and almost no homogeneous flow exits.

6. Conclusions

This work presents a three-dimensional kinematically admissible velocity field for the extrusion of a hexagonal three-layer composite clad rod. Also examined herein are factors that dominate the deformation pattern of the rod, including the semi-die angle, friction on the die surface, the strength combinations of the constituent materials and the reduction of area of the billet. Based on the results presented herein, the following can be concluded.

1. For a semi-die angle between 10° and 20°, the extrusion pressure required is the lowest.
2. A higher frictional factor promotes a non-uniform velocity distribution in the extrusion direction (β_s increases).
3. Combining the three-layer composite clad rod with the hardest core/softest sleeve is highly desirable for extrusion.
4. The proposed model can be applied to the extrusion of a composite clad rod with an irregular cross-section if a function can mathematically express its cross-sectional profile.

References

[1] K. Osakada, M. Limb, P.B. Mellor, Hydrostatic extrusion of composite rods with hard cores, Int. J. Mech. Sci. 15 (1973) 291–307.
[2] J.M. Story, B. Avitzur, W.C. Hahn, The effect of receiver pressure on the observed flow pattern in the hydrostatic extrusion of bimetal rods, ASME J. Eng. Ind. 98 (3–4) (1976) 909–913.
[3] B. Avitzur, R. Wu, S. Ralbert, Y.T. Chou, Criterion for the prevention of core fracture during extrusion of bimetal rods, ASME J. Eng. Ind. 104 (1982) 293–304.
[4] B. Avitzur, R. Wu, S. Ralbert, Y.T. Chou, Criterion for the prevention of sleeve fracture during extrusion of bimetal rods, ASME J. Eng. Ind. 104 (1986) 205–212.
[5] W. Zoerner, A. Austen, B. Avitzur, Hydrostatic extrusion of hard core clad rod, ASME J. Eng. Ind. 94 (1972) 78–80.
[6] M. Kiuchi, S. Itoh, Limit analysis of drawing and extrusion of composite material 1st report, Seisan-KenKyu 31 (2) (1979) 763–766.
[7] M. Kiuch, R.Q. Hsu, Numerical simulation of drawing of multi-cores clad rods, Ann. CIRP 39 (1990) 271–274.
[8] C.W. Wu, R.Q. Hsu, Theoretical analysis of extrusion of rectangular, hexagonal and octagonal composite clad rods, Int. J. Mech. Sci. 42 (2000) 473–486.
[9] W.G. Wang, H.K. Liu, Y.C. Guo, P. Bain, S.X. Dou, Mechanism of deformation and "sandwich" rolling process in Ag-clad Bi-base composite tapes, Appl. Superconduct. 3 (1995) 599–605.
[10] J. Jeng, C.W. Wu, R.Q. Hsu, Extrusion of three-layer composite clad rods, Australiasia-Pacific Forum Intell. Process. Manuf. Mater. 2 (1997) 864–871.